

Cosmological constraints from the cluster contribution to the power spectrum of the soft X-ray background. New evidence for a low σ_8

J.M. Diego¹, W. Sliwa², J. Silk¹, X. Barcons³, W. Voges⁴

¹ *University of Oxford, Denys Wilkinson Building, 1 Keble Road, Oxford OX1 3RH, United Kingdom.*

² *Nicolaus Copernicus Astronomical Center, Bartycka 18, 00-716 Warsaw.*

³ *Instituto de Fisica de Cantabria (CSIC-UC), 39005 Santander, Spain.*

⁴ *Max-Planck-Institut für extraterrestrische Physik, 85741 Garching, Germany.*

Draft version 1 November 2018

ABSTRACT

We use the X-ray power spectrum of the *ROSAT* all-sky survey in the R6 band ($\approx 0.9\text{--}1.3$ keV) to set an upper limit on the galaxy cluster power spectrum. The cluster power spectrum is modelled with a minimum number of robust assumptions regarding the structure of the clusters. The power spectrum of *ROSAT* sets an upper limit on the $\Omega_m - \sigma_8$ plane which excludes all the models with σ_8 above $\sigma_8 = 0.5\Omega_m^{-0.38}$ in a flat Λ CDM universe. We discuss the possible sources of systematic errors in our conclusions, mainly dominated by the assumed $L_x - T$ relation. Alternatively, this relation could be constrained by using the X-ray power spectrum, if the cosmological model is known. Our conclusions suggest that only models with a low value of σ_8 ($\sigma_8 < 0.8$ for $\Omega_m = 0.3$) may be compatible with our upper limit. We also find that models predicting lower luminosities in galaxy clusters are favoured. Reconciling our cosmological constraints with these arising by other methods might require either a high entropy floor or wide-spread presence of cooling flows in the low-redshift clusters.

Key words: cosmological parameters, galaxies:clusters:general

1 INTRODUCTION

Galaxy clusters are a useful probe of cosmological models. In recent years there has been a wide variety of work based on the study of the population of galaxy clusters as a way to constrain cosmological models. The mass function derived from N-body simulations as well as analytical approaches like the Press-Schechter mass function show a strong dependence of the mass function on the cosmological model. By using the local abundance of clusters, it is possible to set strong constraints on the $\sigma_8 - \Omega_m$ plane.

However, both parameters are degenerate and one needs to go to higher redshifts in order to break this degeneracy. Combining the low redshift mass function with the high redshift mass function it is possible to break the degeneracy in $\sigma_8 - \Omega_m$ and determine both parameters (Bahcall & Fan 1998). Nevertheless, a measurement of the mass function (especially at high redshift) is very difficult to achieve since the mass of a cluster cannot be measured directly but requires modelling of the observations. Direct measurement of the mass requires the use of sophisticated techniques such as gravitational lensing (and high quality data) or tracing the mass via the X-ray emission under the assumption of hydrostatic equilibrium.

An alternative approach can be devised by transforming masses into temperatures or luminosities and using the equivalent temperature function or luminosity function instead of the mass function. The drawback of this last approach is that in this case a $T - M$ relation or a $L_x - M$ relation needs to be assumed. These scaling relations suffer from scatter and they are not yet very well established. Even in the case where these relations are well known, there are still several systematic effects which are difficult to be accounted for. For instance, the luminosity of a cluster depends on the cosmological model since luminosities are obtained from the measured flux times the square of the luminosity distance. In the case of X-rays, the X-ray emission is concentrated in the centre of the cluster (due to the n^2 dependence with n being the electron density) and most of the emission coming from the external parts of the cluster is not detected. In order to compute the total luminosity of the cluster one needs to assume a profile for the electron density and extrapolate the observed emission to the outer parts. When using the mass, temperature, flux or luminosity functions in cosmological studies, a precise knowledge of the selection function of the survey is required since the observed function will be compared with the theoretical one in which the integration

Figure 1. ROSAT all-sky survey (RASS) map in the R6 band in galactic coordinates. The map has been repixelized using HEALPIX. The colour scale is logarithmic and the units are $10^{-6} \text{ cts/s arcmin}^2$. The two horizontal lines mark the two constant Galactic latitudes at $|b| = 40^\circ$. The thick lines show the galactic meridians $l = 70^\circ$ (left) and $l = 250^\circ$ (right).

of the mass (or temperature, flux, luminosity) starts at a minimum value (as a function of z) defined by the selection function of the survey. Usually this selection function is inhomogeneous due, e.g., to different exposures in different sky directions. This makes the modelling of the theoretical mass (temperature, flux or luminosity) function very complicated. Also due to the selection function of the survey, the number of clusters observed (i.e. detected above some detection threshold) represents only a small fraction of the population of clusters. This means that cosmological studies based on the mass (temperature, flux or luminosity) function are based only on the *tip of the iceberg* and therefore subject to large variations due to small number statistics.

In this work we propose the use of the power spectrum as an alternative cosmological test which is less affected by the problems pointed out above. Our attempt is not to measure the power spectrum of galaxy clusters (see for instance Schuecker et al. 2001) but to use the power spectrum of the diffuse X-ray background as an upper limit (see Fabian & Barcons 1992 for a discussion of the X-ray background). This approach has several advantages over previous work.

(i) First, since we use the diffuse power spectrum as an upper limit, we do not need to *detect* the clusters. The only thing we need to do is to model the X-ray cluster power spectrum and compare it with the measured one. The cluster power spectrum must remain below the one due to the global fluctuations of the diffuse cosmic X-ray background (Barcons & Fabian 1988, Carrera et al. 1997, Barcons et al. 1998, Yamamoto & Sugiyama 1998).

(ii) In modelling the cluster power spectrum we do not need to know the selection function since all the clusters (detected and undetected) will contribute to the power spectrum.

(iii) The previous point has a very interesting feature. We are not only sensitive to the tip of the iceberg but to the whole iceberg itself! This fact has interesting applications in studies like pre-heating (see e.g. Voit et al. 2002) which are particularly important in the low-mass regime where clusters are difficult to detect.

(iv) Since we do not need to detect the individual clusters we are not affected by any extrapolation of the measured flux (needed to get the total luminosity or mass) making our results more independent of the assumed profile of the clusters.

(v) The power spectrum is scale dependent. Previous work has used the energy spectrum as an upper limit to constrain the emission from galaxy clusters (see e.g. Wu et al. 2001). However, in these studies the measured emission is contaminated by the diffuse emission coming from the Galaxy. This is equivalent to studying just the monopole of the multipole decomposition. On the contrary, the power spectrum can disentangle the diffuse from the point-source emission since the diffuse emission will contribute significantly only to the large scales (low multipoles) while the emission from point-sources will dominate the smaller scales (intermediate-high

multipoles).

In the next sections we will describe briefly the power spectrum of RASS diffuse emission (section 2), we will define the model to compute the cluster power spectrum (section 3) and we will constrain the cosmological model (section 4). In section 5 we revise the assumptions made in the previous sections and check how the results change when we change the model. Finally, we discuss our results in section 7 and summarise in section 8. Throughout the paper (unless otherwise stated), the Hubble constant is given as $100 h \text{ km s}^{-1} \text{ Mpc}$.

2 THE POWER SPECTRUM OF ROSAT

The use of the spherical harmonics decomposition of the intensity of the X-ray background as a means to measure or constrain cosmological parameters was first proposed by Lahav, Piran & Treyer (1997). The emphasis was mostly on the contribution of the clustering of point sources (mostly AGNs). They focused their analysis on the low multipoles ($l < 10$). That sort of study has the disadvantage that the physics that leads to the formation and clustering of these exceptional sources is not simple and it is hidden in an unknown *bias* parameter. Indeed, Treyer et al. (1998) conducted that analysis on the 2-10 keV data from the HEAO-1 A2 experiment and found some interesting constraints on the bias parameter of X-ray sources, but no direct implications on the cosmological parameters themselves. The use of a softer band (but not heavily contaminated by the Galaxy) to constrain the cluster power spectrum and derive cosmological parameters is a much more promising task, as the physics of the cluster formation is much simpler and closer to the Cosmological model.

The harmonic power spectrum of the diffuse *ROSAT* All-Sky Survey (RASS, see Snowden et al. 1997) X-ray background has been computed up to $l \approx 1000$ in a previous work (Sliwa et al. 2001). In that work the authors computed the power spectrum in different areas (subsamples) of the sky centred in the north pole. They also studied the effects of the data binning in pixels and calculated the error estimates due to limited counting statistics, instrumental background subtraction, and cosmic variance.

On the other hand, the power spectrum of clusters in X-rays has been recently measured using *ROSAT* data (see Schuecker et al. 2001 for an estimation based on the REFLEX survey and Borgani et al. 1999 for an estimation of its Fourier transform, the two point correlation function, from the XBACs cluster sample). That measured cluster power spectrum has been also used to constrain the cosmological model (Schuecker et al. 2002). In that work, the modelling of the observed cluster power spectrum (above certain lim-

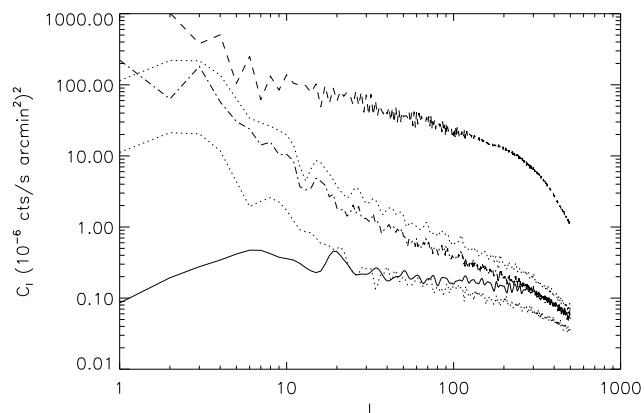


Figure 2. *ROSAT* power spectrum in the R6 band computed with HEALPIX in different areas of the sky. Top dashed line C_l , for the all-sky RASS data. Dotted lines, C_l for the fraction of the sky with $b > 40^\circ$ (top) and $b < -40^\circ$ (bottom). Dot-dashed line, C_l for the part of the sky defined by $|b| > 40^\circ$ and thick solid line, C_l for the optimal area: $l \in [70^\circ, 250^\circ]$ and $b > 40^\circ$ (equal to sample D in Sliwa et al. 2001). The power in this area does not show a significant galactic contamination. Our estimations are comparable to the ones obtained in Sliwa et al. (2001).

iting flux) is a complicated procedure which involves several assumptions (such as the $L_x - M$ relation which was taken from Reiprich & Böhringer 2002). Results obtained in a different study (Viana et al. 2002) seem to indicate that there could be an inconsistency between the REFLEX luminosity function and the $L_x - M$ relation obtained by Reiprich & Böhringer (2002).

In this work, instead of detecting clusters and finding the power spectrum from the sample of detected clusters, we will use the RASS power spectrum to set an upper limit on the cosmological model. This approach has several advantages outlined in the previous section. In brief, we recall that the main advantage of this work will be a better control of the systematic errors.

We have re-estimated the power spectrum in an independent way (compared with the estimation of Sliwa et al. 2001). In our process, we have repixelized the RASS data using the package HEALPIX^{*} and computed the power spectrum with the same package. HEALPIX was originally designed to analyse mega-pixel CMB data and is optimised for the computation of the harmonic power spectrum.

The pixel size of the RASS maps is 12 arcmin and the maps are given in different bands. We choose the band R6 which is the one in which the cluster signal is expected to be at its maximum compared to the other components (local bubble, galactic diffuse emission, extragalactic AGN's). This band is also the best in terms of the instrumental response and background contamination. We repixelise the RASS in HEALPIX using a pixel size of ≈ 13.7 arcmin ($N_{\text{side}} = 256$) and compute the power spectrum with the HEALPIX sub-

routine anafast. $N_{\text{side}} = 256$ gives the closest HEALPIX pixelisation to the original *ROSAT*'s one. Due to the large pixel size, we can compute the power spectrum up to only $l = 500$. Beyond that point we do not have information about smaller scales. With this pixel size, the effect of the PSF of *ROSAT* becomes negligible and we will not include it in our analysis. However, at smaller scales, the *ROSAT* PSF can have an important effect on the measured power spectrum.

In figure 1 we show the RASS data in the R6 band after repixelisation with HEALPIX. Several features can be observed in the map, the most prominent one being the Galactic plane. The diffuse X-ray maps used in this work have been cleaned of the most prominent point sources (see Snowden et al. 1997). The brightest point sources (Voges et al. 1999, Voges et al. 2000) were removed making use of the full resolution of the PSPC detector ($1.6' \times 1.6'$ pixel size) using a minimum source-excision radius of $3.5'$. 50000 sources were removed above a threshold of 0.02 cts/s in the R6+R7 band. Below this threshold, there are still many point sources which could contribute to the power spectrum. In the maps, there are several strips with no data (black bands in figure 1). There are also many pixels with 0 count-rate, specially in the southern hemisphere.

We are interested in computing an estimate of the power spectrum in an area of the sky which is large enough to avoid cosmic variance fluctuations but also that has a low foreground contamination and low noise level. The contamination level is determined basically by the amount of Galactic emission. We should then avoid regions with strong galactic emission. The noise level is determined by the exposure time. We should then concentrate on those regions having low galactic emission and large integration times. We have selected a region with $b > 40^\circ$ and $l \in [70^\circ, 250^\circ]$ (totalling ≈ 2400 deg²) as the optimal region for our analysis (see figure 1). Several groups have selected also this region for their studies of the X-ray background (Soltan et al. 1996, Miyaji et al. 1996, Kneissl et al. 1996, Sliwa et al. 2001).

In figure 2 we show the power spectrum in different areas of the sky. We have represented the power spectrum in different situations where we exclude (or include) the galactic plane ($|b|$ above or below 40°). The galaxy contributes on large scales (low l 's) but also introduces power at intermediate l 's. The power spectrum calculated in our optimal area is shown as a thick solid line. In this case, no structure due to the Galaxy is seen, suggesting that this area may be dominated by the cosmological signal (galaxy clusters and faint AGNs). The optimal area has also a very low N_H column density, typically $\sim 2 \times 10^{20}$ cm⁻². The absorption of the X-ray flux by this column density is only a few percent in most of the pixels in this area, an effect that can be safely neglected.

3 THE CLUSTER POWER SPECTRUM

We have used the halo model to compute the power spectrum due to galaxy clusters (Cole & Kaiser 1988, Bartlett & Silk 1994, Komatsu & Kitayama 1999, White 2001, Cooray 2002, Komatsu & Seljak 2002). In this model, the power spectrum is due to two main contributions, the two-halo con-

^{*} available at <http://www.eso.org/science/healpix>. Copyright 1997 by Eric Hivon and Krzysztof M. Gorski. All rights reserved.

tribution and the single-halo contribution. The first one includes the correlation between clusters and only contributes significantly in the very large scale regime. The single-halo contribution accounts for the individual contribution of each cluster to the power spectrum and dominates at smaller scales.

The large scales (low l) of the power spectrum in the optimal area may be affected by window effects and cosmic variance (our optimal area is just $\approx 9\%$ of the sky). Although the power spectrum in the optimal area seems to be free of galactic contamination, it may happen that the galaxy is still contributing in this area. For all these reasons, the low l regime should be excluded in our cosmological analysis. We will concentrate only on the intermediate-small scales for which one can consider only the single-halo contribution and neglect the two-halo contribution.

However, we should keep in mind that, as noted in Komatsu & Kitayama (1999), the clustering contribution can amount to 20% – 30% of the single halo-contribution at degree angular scales ($l \approx 100$) (see also Lahav et al. 1997 for smaller multipoles). Therefore, by neglecting the two-halo contribution we are being conservative in our assumptions. The real power spectrum of galaxy clusters will be about 20% – 30% larger than the one considered in this work.

The single-halo contribution is just an integrated effect over redshift of the individual contribution from each cluster.

$$C_l = \int dz \frac{dV(z)}{dz} \int dM \frac{dN(M, z)}{dM} p_l(M, z) \quad (1)$$

where $dV(z)/dz$ is the volume element, $dN(M, z)/dM$ is the cluster mass function and $p_l(M, z)$ is the power spectrum (multipole decomposition) of the X-ray 2D profile of the cluster with mass M at redshift z . In this work we have assumed the Press-Schechter approach for the mass function (Press & Schechter 1974) and we use a numerical fit to the multipole decomposition of the X-ray 2D profile as we will describe in the next subsection.

3.1 The multipole decomposition of the X-ray 2D profile

Since the power spectrum of galaxy clusters is proportional to the square of the density profile, it is important to be careful in the selection of this profile and make the *safest* assumptions about it. The usual approach is to consider a numerical model for the electron density profile (a β -model or a numerical fit to N-body simulations) and compute the flux from the integrated signal of the profile. Then, assume isothermality of the plasma and some relation between the mass of the cluster and its temperature. In this process there are several *dangerous* steps. Assuming a bremsstrahlung spectrum, the monochromatic volume emissivity of the intra-cluster medium scales as $j_\nu \propto n^2/\sqrt{T}$, where n is the electron density and T its temperature. Then the integrated bolometric luminosity scales as the square of the central density times the square root of the temperature (assuming the cluster is isothermal). The central density has been poorly estimated so far in galaxy clusters and there is a lot of uncertainty in its typical value. If the cluster is assumed to be isothermal and the scaling relation between mass and temperature is taken to be the one predicted by

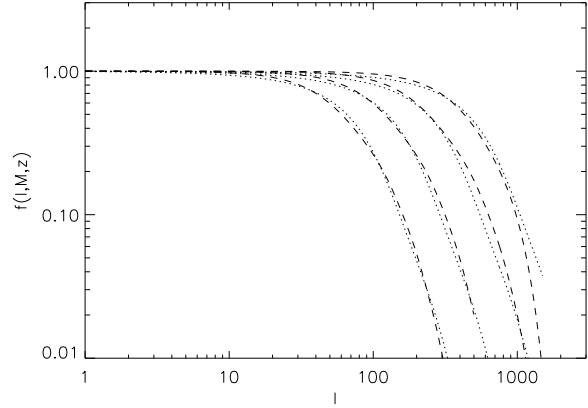


Figure 3. Multipole decomposition of the 2D X-ray profile for different core radii (r_c). From left to right. $r_c = 27, 13.7, 7, 3.5$ arcmin. The dashed line represents the real multipole decomposition and the dotted line is the numerical fit of equation 5.

the spherical collapse model, one ends up with a $L_x - T$ relation which is inconsistent with recent observations. We can conclude that, modelling of the X-ray emission in galaxy clusters from numerical models can be a quite unsafe process. It is more useful to formulate the model in terms of observational quantities rather than theoretical models which fail in explaining the observations.

Basically what we need for our model is just an expression of the form;

$$p_l(M, z) = p_o(M, z) * f(l, M, z) \quad (2)$$

where p_o is the normalisation and $f(l, M, z)$ contains the angular dependence of the multipole decomposition. To understand why this simple form will suffice, it is useful to think in terms of a single point source. This source will have a constant power spectrum ($f(l, M, z) = 1$) and a normalisation which is equal to;

$$p_o(M, z) = 4\pi |Mean|^2 = 4\pi \left| \frac{S_T}{4\pi} \right|^2 \quad (3)$$

where $Mean$ is the total signal, S_T , divided by the area of the sky. In the case of a cluster, the situation is similar except that in this case the source will be extended and $f(l, M, z)$ will not be constant anymore. In this case, we have to assume a profile for the electron gas. We assumed a β -model (with $\beta = 2/3$) profile for the electron cluster density. This assumption is supported by a wealth of observational data. We also have truncated the profile at the virial radius defined as $r_v = pr_c$ with p a fixed parameter ($p \approx 10$) and r_c the core radius.

$$n(r) = \frac{n_o}{1 + (r/r_c)^2} \quad (4)$$

Instead of fixing the central density, n_o , we will fix the total luminosity so the value of n_o will be irrelevant in our model. The only free parameter is the core radius, r_c . This will be an advantage compared to other works since we can make our model consistent with real observations rather than with simulations.

To compile an expression for the multipole dependence of the

2D profile, we have computed $f(l, M, z)$ for different clusters changing the only free parameter, r_c , and then fitting the result to an analytical form. The best fit we found is;

$$f(l, M, z) = \frac{1}{2} \left(\exp(-\xi_{l,r_c}) + \exp(-\sqrt{\xi_{l,r_c}}) \right) \quad (5)$$

with,

$$\xi_{l,r_c} = l^2 r_c^{1.5/(0.815+0.35r_c)} \quad (6)$$

where the core radius, r_c , is given in rads (see figure 3). The mass and redshift dependence of $f(l, M, z)$ is in r_c .

$$r_c = \frac{r_o}{p} M^{1/3} (1+z) \quad (7)$$

Although we have assumed the expected redshift dependence of the self-similar spherical collapse model with $\Omega_m = 1$, we will adopt this form for simplicity. As we will show below, the power spectrum of galaxy clusters will be dominated by the low redshift population for which the specific form of the redshift dependence is not very important. The value of r_o must be assumed and we should keep in mind that typical core radii for massive clusters are around 100 kpc. We will adopt a value of $r_o/p = 130 h^{-1}$ kpc for a mass of $M = 10^{15} h^{-1} M_\odot$ at redshift 0 and will discuss other values later.

Regarding the normalisation of the profile, p_o , we only have to determine *Mean*, that is, the total signal divided by the area of the sky. To avoid systematic effects due to unrealistic modelling based on simulations, we have parametrised the total signal in terms of observed quantities, like the $L_x - T$ relation. We used the scaling relations derived in Diego et al. (2001). In that work, the authors made a consistent fit to the mass function, temperature function, X-ray flux function and X-ray luminosity function. In the fit both, the cosmological model, and the cluster scaling relations were considered as free parameters and were fitted to the data. Using the $L_x - T$ relation we can obtain the total signal (flux) of the cluster, S_T , from its temperature.

$$S_T = f_c \frac{L_x}{4\pi D_l(z)^2} = f_c \frac{L_o T_{keV}^\alpha (1+z)^\psi}{4\pi D_l(z)^2} \quad (8)$$

where we use the values of L_o , α and ψ obtained in Diego et al. (2001) ($L_o = 1.12 \times 10^{42} h^{-2} \text{erg/s}$, $\alpha = 3.2$ and $\psi = 1$ for a flat Λ CDM universe). The temperature is obtained using the $T - M$ relation found in Diego et al. (2001) ($T_{keV} = 9.48 M_{15}^{0.75} (1+z)$). This relation is different from the best fitting function to the observed $T - M$ relation (see e.g. in Nevalainen et al. 2000). However, we will use this relation to be consistent with the above $L_x - T$ relation and the constraints in Diego et al. (2001). In section 6 we will discuss other (possibly more realistic) alternatives.

We should note that by changing the parameters L_o , α and ψ we can include also the uncertainty in the $T - M$ relation into an uncertainty in the $L_x - T$ relation. That is, the parameters L_o , α and ψ will somehow mimic variations in the parameters of the $T - M$ relation. This choice is not arbitrary. We could easily model the total luminosity as a function of mass and use the $L_x - M$ relation as our *free-parameter* scaling relation. However, we prefer to parametrise our model in terms of the $L_x - T$ relation since it is observationally better constrained than the $L_x - M$ relation.

The only free parameters in our model are then the $L_x - T$ relation and the r_c modelling. We will study their effect

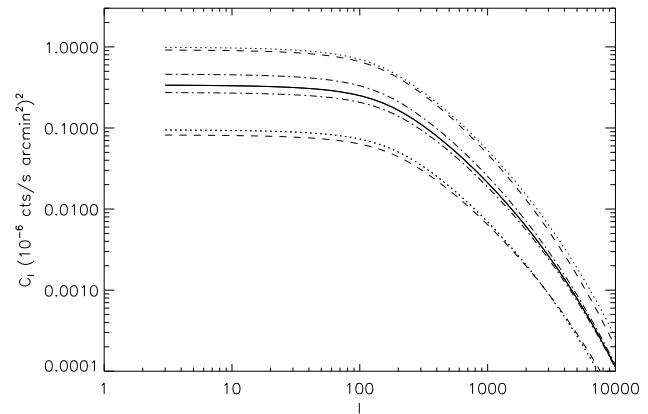


Figure 4. Dependence of the X-ray power spectrum on the cosmological parameters σ_8 , Ω and Γ . The solid line is the reference model ($\sigma_8 = 0.8$, $\Omega_m = 0.3$ and $\Gamma = 0.2$). We show the effect of changing one of the three parameters while keeping unchanged the other two. The effect of changing σ_8 while Ω and Γ are fixed to the values of the reference model is shown in the dotted lines. Bottom dotted line is for $\sigma_8 = 0.7$ and top dotted line is for $\sigma_8 = 0.9$. Dashed lines show the effect of changing Ω_m in 0.1 units. Bottom dashed line is for $\Omega_m = 0.2$ while the upper dashed line is for $\Omega_m = 0.4$. Finally, the dot-dashed lines show the effect of changing the shape parameter, Γ . Bottom dot-dashed line is for $\Gamma = 0.25$ and upper dot-dashed line for $\Gamma = 0.15$

later.

The factor f_c is the conversion factor between $\text{erg cm}^{-2} \text{s}^{-1}$ to $10^{-6} \text{cts/s arcmin}^2$ which are the units in which the RASS data are given. We compute this factor with the X-ray package XSPEC (Arnaud 1996). We have assumed a *z-bremsstrahlung* model and considered only the *ROSAT* PSPC channels of the R6 band (channels 91-131, see Snowden et al. 1997). The *ROSAT* response was modelled using the response matrix file of the detector PSPC-C. Using a Raymond-Smith for the model spectrum with 0.3 solar metallicity in the R6 band does not introduce a significant difference compared to the *z-bremsstrahlung*. The *K*-correction was also included in the factor f_c . This factor was computed for each temperature and redshift.

As an example, XSPEC predicts a conversion of $1 \text{ cts/s} = 8.6 \times 10^{-12} \text{ erg/s cm}^{-2}$ in the R6 band (for $kT = 7 \text{ keV}$ and $z = 0.5$)

3.2 Cosmological dependence of C_l

The power spectrum shows an important dependence with the cosmological parameters σ_8 , Ω and Γ . In figure 4 we show some examples where we vary the normalisation of the power spectrum, σ_8 , the matter density, Ω , and the shape parameter, Γ . The dependence with σ_8 and Ω is very important. A change of 0.2 units in Ω leads to a change in the power of one order of magnitude. Something similar happens with σ_8 although in this case the change is slightly weaker. The dependence on Γ is not so important. In particular, in our region of interest ($l \approx 100$), Γ does not have a very significant effect on the power spectrum. For this reason we

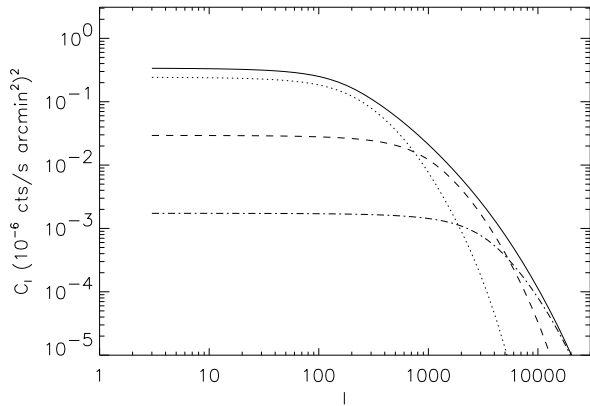


Figure 5. Power spectrum of galaxy clusters (with $M \in [3 \times 10^{13}, 10^{16}]h^{-1}M_{\odot}$) split in different redshift intervals ($\sigma_8 = 0.8$, $\Omega_m = 0.3$). Solid line $z \in [0.01, 2]$, dotted line $z \in [0.01, 0.05]$, dashed line $z \in [0.05, 0.2]$ and dot-dashed line $z \in [0.2, 2]$.

will fix Γ in our analysis to its most favoured value $\Gamma = 0.2$ (from 2dF, Percival et al. 2001) and we will vary only σ_8 and Ω_m .

3.3 Mass and redshift dependence of C_l

Before comparing the cluster power spectrum with the *ROSAT* data in the R6 band, it is interesting to look in more detail at the way the different cluster populations contribute to the power spectrum. Given a cosmological model, the cluster mass function is just a function of two variables, mass and redshift. We can now examine the cluster population at different mass and redshift intervals to find out which regimes dominate at different scales.

Low redshift clusters will dominate the large scales since at low redshift the clusters appear larger (figure 5). Also, it is difficult to find large clusters at high redshift. They usually appear at low z . On the contrary, high redshift clusters will dominate the high- l regime. At high z , clusters will appear with small angular scales. Also, the typical mass of a cluster decreases with redshift. However, clusters beyond $z \approx 0.2$ will contribute only at the very small scales ($l > 2000$ or scales smaller than ≈ 5 arcmin). At scales larger than 5 arcmin, only the clusters below $z \approx 0.2$ are relevant in the power spectrum. We also show the contribution in the range $z \in [0.01, 0.05]$. Many Abell clusters will contribute to this part of the power spectrum (min $z_{Abell} \approx 0.01$).

In terms of the masses (figure 6), the power spectrum is dominated by intermediate mass clusters (dashed line). The very massive clusters are rare and they do not dominate the power spectrum at any scale. They are big clusters and usually appear at low redshift. As a consequence, they will contribute significantly only to the large scales. On the contrary, intermediate-mass clusters are common in a wider range of redshifts and their integrated signal dominates the signal of the very massive clusters. The intermediate-mass clusters are bright enough to dominate the power spectrum at practically all scales. Finally, the low-mass clusters will contribute only to the very small scales (high l -s). They are

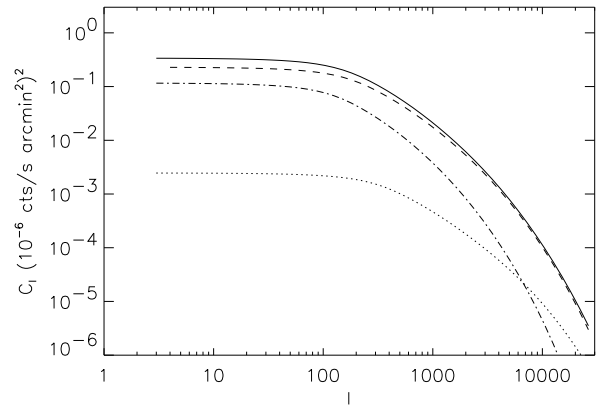


Figure 6. Power spectrum of galaxy clusters (with $z \in [0.01, 2]$) split in different mass intervals ($\sigma_8 = 0.8$, $\Omega_m = 0.3$). Solid line $M \in [3 \times 10^{13}, 10^{16}]h^{-1}M_{\odot}$. Dotted line shows the contribution of the *dark clusters*, $M \in [3 \times 10^{13}, 10^{14}]h^{-1}M_{\odot}$. Dashed line shows the dominant contribution of the intermediate-mass clusters, $M \in [10^{14}, 10^{15}]h^{-1}M_{\odot}$ and the dot-dashed line shows the contribution of the very massive clusters, $M \in [10^{15}, 10^{16}]h^{-1}M_{\odot}$.

more abundant than the intermediate-mass clusters but the signal is weaker.

Combining the results of figures 5 and 6 we can conclude that the cluster power spectrum up to $l \approx 500$ will be dominated by the cluster population with $z < 0.2$ and intermediate masses, $M \in [10^{14}, 10^{15}]h^{-1}M_{\odot}$. This can be seen more clearly in figure 7 where we present the differential contribution to different multipoles as a function of mass (lower set of curves) and redshift (upper set of curves). For representation purposes, all the power spectra has been normalised to 7 for the redshift case and to 4 for the mass case.

4 CONSTRAINTS ON $\sigma_8 - \Omega_M$

After computing the power spectrum from eqn. 1 for hundreds of models where we change σ_8 and Ω , we can compare the predicted power spectrum with the observed RASS power spectrum in the R6 band and exclude all the models for which we have more predicted power than the observed one. We show the result in figure 8. The dotted line is a numerical fit to the upper limit.

$$\sigma_8 = 0.5\Omega_m^{-0.38} \quad (9)$$

Our limit excludes regions in the $\sigma_8 - \Omega_m$ plane which are within the confidence region of many other methods. In figure 9 we compare the RASS power spectrum with three models above, on, and below the upper limit curve ($\sigma_8 = 0.75, 0.8, 0.85$, for $\Omega = 0.3$). The range of l 's which exclude the models above the upper limit are up to $l \approx 200$ which corresponds to angular scales $\theta \approx 1^\circ$. At these scales only the nearby clusters (like the Abell clusters) contribute to the power spectrum (see figure 5 and 6). Hence, with this data we are not very sensitive to the population of clusters at moderate and high-redshift. This fact is in agreement with the measured cross-correlation between the angular position

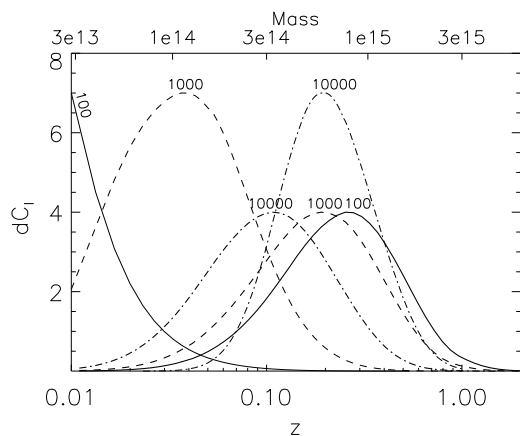


Figure 7. Differential contribution to different multipoles as a function of redshift (top curves) and mass (thick bottom curves). Solid line is the contribution to the multipole $l = 100$, dashed line for $l = 1000$ and dot-dashed for $l = 10000$. All the curves have been normalised to 7 (top) and 4 (bottom). The numbers on top of the curves indicate the multipole to which they are contributing. The mass scale is shown in the upper x-axis and the z -scale in the bottom x-axis.

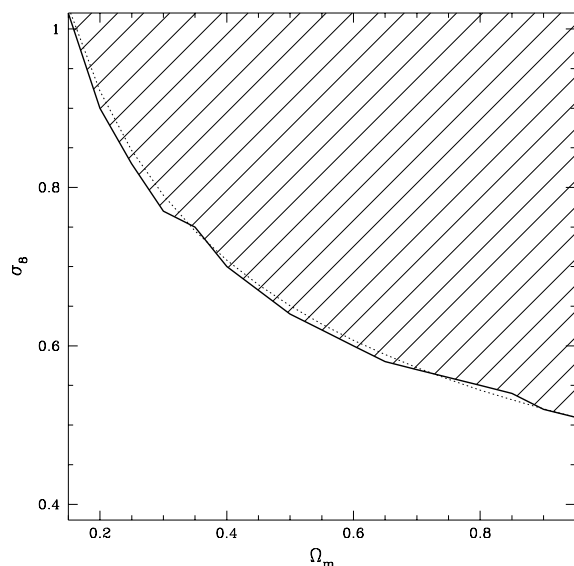


Figure 8. Upper limit constraints in the $\sigma_8 - \Omega_m$ plane (solid line). The dotted line corresponds to the curve, $\sigma_8 = 0.5\Omega_m^{-0.38}$.

of Abell clusters and the intensity of the X-ray background (Soltan et al. 1996). In that work, the authors found that the cross-correlation extends up to several degrees (*i.e.* the cluster–X-ray background cross-correlation spreads over the range $l < 100$).

The RASS data still contains some contribution of non-removed point sources which could be contaminating the power spectrum at sub-degree scales. This fact suggests that a study carried out on a smaller region of the sky with a more careful point source removal could render better con-

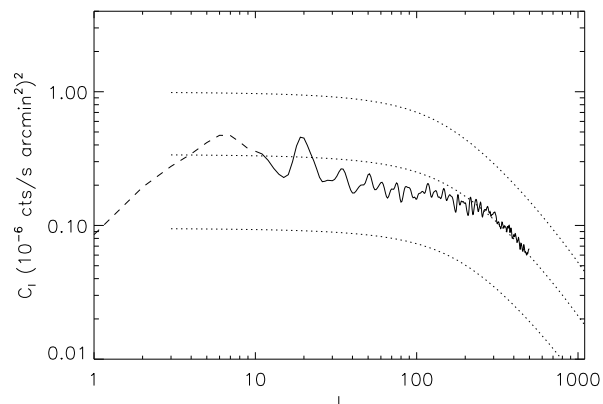


Figure 9. *ROSAT* power spectrum in the R6 band (solid line) compared with three models above and below the upper limit (dotted lines). From top to bottom, $\sigma_8 = 0.7$, $\sigma_8 = 0.8$ and $\sigma_8 = 0.9$. All models are for $\Omega_m = 0.3$. The dashed line part of the *ROSAT* power spectrum was not used in the calculation of the upper limit in figure 8.

straints on the cosmological model. This opens an exciting possibility for future work carried out with *Chandra* and/or especially with XMM-Newton data. XMM-Newton has a higher sensitivity for extended sources and wider field of view than *Chandra*. This makes XMM an ideal instrument for wide field X-rays surveys (like the XMM-LSS, Refregier et al. 2002a). However, the analysis of the arcmin-subarcmin scales is beyond the scope of this paper and will be discussed in a subsequent paper.

The constraints derived in this section are robust since they were obtained under a minimum number of assumptions.

However, variations in these assumptions ($L_x - T$, core radius) can have an important effect on the resulting power spectrum. It is important to study how the upper limits obtained in this section can be affected by varying our assumptions ($L_x - T$ relation and core radius, r_c). Although the model we assumed for $L_x - T$ and core radius was consistent with several optical and X-ray cluster data sets (as shown in Diego et al. 2001), there are some uncertainties in the values of the parameters assumed in the model (L_o , α , ψ and r_c). A different set of values for these parameters will render a different upper limit on the $\sigma_8 - \Omega_m$ plane. Our results can be therefore affected by systematic errors due to the wrong election of the parameters of the model. In the next section we will attempt to see how much does our upper limit change when we make different assumptions in our model.

5 SYSTEMATIC EFFECTS

The main source of possible systematic error is the normalisation of the assumed $L_x - T$ relation, L_o (eqn. 8). There is still an important uncertainty in this relation and even a break could be present at low temperatures. This break in

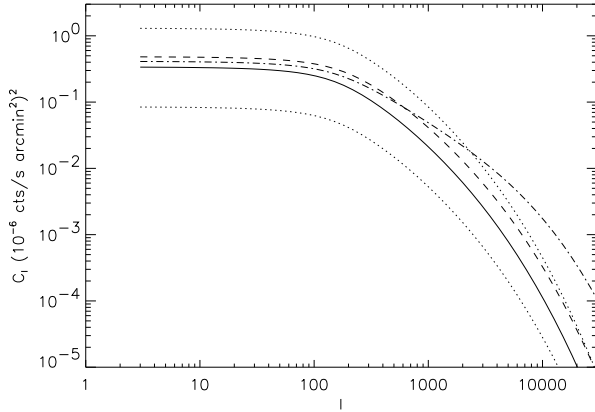


Figure 10. Systematic effects. Effect of changing L_o , α and ψ in the $L_x - T$ relation (eqn. 8) for a $\sigma_8 = 0.8$, $\Omega_m = 0.3$ model. The thick solid line is the reference model. ($L_o = 1.12 \times 10^{42} h^{-2} \text{erg/s}$, $\alpha = 3.2$, $\psi = 1$). The dashed line correspond to the same value of L_o but $\alpha = 2.7$. The dotted lines are for $L_o = 2.25 \times 10^{42} h^{-2} \text{erg/s}$ with $\alpha = 3.2$ (top) and $L_o = 0.56 \times 10^{42} h^{-2} \text{erg/s}$ with $\alpha = 3.2$. In the dot-dashed line we fix $L_o = 1.12 \times 10^{42} h^{-2} \text{erg/s}$, and $\alpha = 3.2$ and we change ψ in four units, $\psi = 5$.

the scaling has been interpreted as due to preheating phenomena (e.g. Voit & Bryan 2001, Babul et al. 2002). Since the power spectrum of the clusters is proportional to the square of the total signal (eqn. 3). The power spectrum will be therefore very sensitive to the normalisation of the $L_x - T$ relation (L_o in eqn. 8). This is illustrated in figure 10 where we change L_o by a factor of two and the power spectrum changes by a factor of four (dotted line) as expected. The dependence of the power spectrum on the scaling exponent, α , is not as dramatic as in the case of L_o . When we change α between $\alpha = 3.2$ and $\alpha = 2.7$ the power spectrum changes from the solid line to the dashed line. Finally, the factor controlling the redshift dependence, ψ , is not very relevant up to $l \approx 100$ but at smaller scales ($l > 100$) it can become important since as we discussed in section 3, at the smallest scales the power spectrum is dominated by the high redshift population. The previous plot demonstrates that one must be careful in choosing the $L_x - T$ relation since the results can change significantly.

The second assumption on our model is about the 2D profile. In this case, our only free parameter is the scaling of the core radius, r_c . We will study the effect of changing the core radius by changing the ratio r_o/p in equation 7. The effect of changing the scaling of core radius is only important at small scales (large l). This is not surprising since at low l 's the value of power spectrum is driven only by its normalisation (p_o in equation 2). When we change the parameter p (ratio between the virial and core radius), we observe that clusters with larger p (i.e. smaller core radius when r_o is fixed) have more power at smaller scales (figure 11). This point is interesting since it shows how our constraints on $\sigma_8 - \Omega_m$ are not very sensitive to the cluster's profile. The $L_x - T$ relation will be the main source of uncertainty.

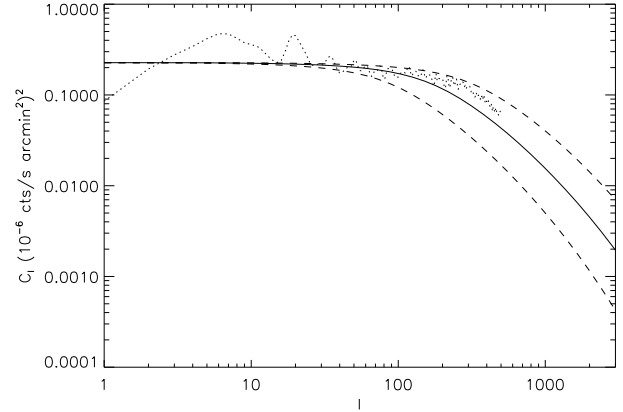


Figure 11. Systematic effects. Effect of changing the parameter p in equation 7 while fixing $r_o = 130 h^{-1}$ Mpc. The solid line is the reference model with $p = 10$ ($\sigma_8 = 0.77$, $\Omega_m = 0.3$). The two dashed lines are for $p = 5$ (bottom) $p = 20$ (top). As expected, clusters which are more extended ($p = 5$) have less power at smaller scales but do not change the power in the large scales (see text). On the other hand, clusters which are more clumped than the $p = 10$ models help to increase the power at smaller scales (without affecting the large scales) and they can produce a good match to the shape of the observed X-ray power spectrum (dotted line) at high multipoles ($\theta < 30$ arcmin). This fact suggests that the clumpiness parameter, p , could be in the range $10 < p < 20$.

From the previous results we can conclude that due to our uncertainty in the $L_x - T$ relation and the cluster density profile (parametrised as a function of r_c) we have an uncertainty in the theoretical power spectrum of clusters of ≈ 1 order of magnitude. We will incorporate this uncertainty in our upper limit in the $\sigma_8 - \Omega_m$ plane by rescaling our theoretical model by a factor of 5 in both directions (multiplication and division). By doing this we will have an *optimistic* and a *pessimistic* model. The optimistic model will contain 5 times more power than the model assumed in section 4 while the pessimistic one will contain 5 times less power. The difference in power between the optimistic and the pessimistic is then a factor 25. The result is shown in figure 12. Even in the pessimistic case, the constraints are still important (models like $\sigma_8 = 1$, $\Omega_m = 0.3$ can be excluded). As an example, the pessimistic case exclude more or less half of the confidence region obtained from the REFLEX cluster power spectrum (see figure 4 in Schuecker et al. 2002).

It is more interesting to see what happens in the optimistic case. Here, models with $\sigma_8 = 0.8$, $\Omega_m = 0.3$ would be excluded. This particular model is actually one of the best in fitting several recent data sets (CMB, 2dF, etc). This means that, if the underlying cosmological model is in fact $\sigma_8 = 0.8$, $\Omega_m = 0.3$, our optimistic case is *too* optimistic! This opens the possibility of using the diffuse X-ray background as a way to study cluster physics rather than constraining the cosmological model. In the hypothetical scenario where the cosmological model is known, one can use the X-ray power spectrum to constrain the physical parameters of the intra-cluster plasma. If, for the *known* cosmology, one observes that the theoretical cluster power spectrum exceeds the observed one, this means that the assumptions made on the

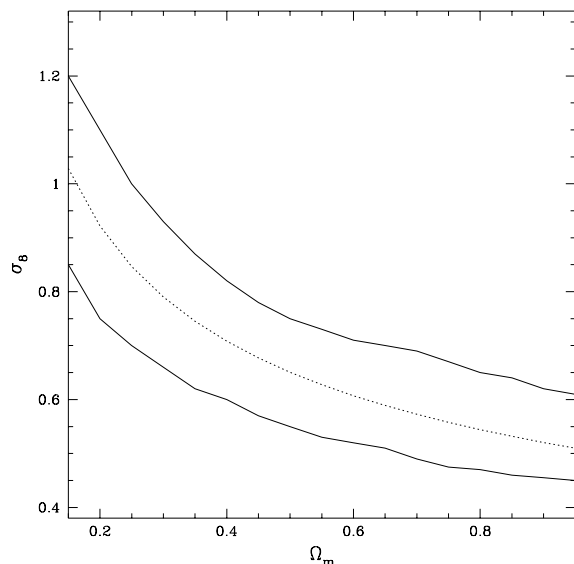


Figure 12. Upper limits constraint in the $\sigma_8 - \Omega_m$ plane for the optimistic (bottom solid line) and the pessimistic (top solid line) models. The dotted line is the numerical fit obtained in section 4 ($\sigma_8 = 0.5\Omega_m^{-0.38}$).

modelling of the cluster power spectrum were wrong (too optimistic case). One should then reintroduce changes in the model in order not to exceed the observed X-ray power spectrum (pre-heating, electron density profile, evolution of the typical luminosity with redshift, baryon fraction, etc)

6 BEYOND THE COSMOLOGICAL MODEL

The main difference between the constraints obtained in this work and those obtained by other methods (based on galaxy clusters) is that we can have a good control on the systematic errors. Our results are not affected by a changing selection function in the sky, or extrapolation of the observed central cluster 2D profile beyond the noise level.

There are only two key assumptions in our model, the $L_x - T$ relation and the cluster density profile. At the scales relevant in this work ($l < 100$) the uncertainty in the cluster density profile is not very important. On the contrary, the main uncertainty comes from our partial knowledge of the $L_x - T$ relation. Most of the *cosmological* methods based on galaxy clusters data obtain the best fitting cosmological model assuming that the physics of clusters are well known. If the uncertainties in the cluster physics are not included, then a biased estimate of the best cosmological model may emerge as a result. We are approaching an era where the best cosmological model is quickly converging to a set of *preferred values*. One can then think the other way around, assuming we know the cosmological model, what can we infer about the physics in clusters ?

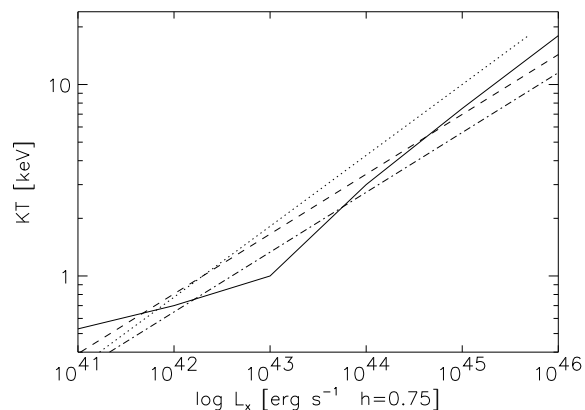


Figure 13. $L_x - T$ relation compared with the pre-heated model (solid line) in Babul et al. (2002). The dashed line represents the main model used in our analysis (figure 8). That model was the best fitting model found in Diego et al. (2001) ($L_o = 1.12 \times 10^{42} h^{-2} \text{erg/s}$, and $\alpha = 3.2$, see eqn. 8) after fitting the cluster mass function, temperature function, X-ray luminosity function and X-ray flux function. Also shown are two of the models used in figure 10. Dotted line is for $L_o = 1.12 \times 10^{42} h^{-2} \text{erg/s}$, and $\alpha = 2.7$, and dot-dashed line is for $L_o = 2.25 \times 10^{42} h^{-2} \text{erg/s}$, and $\alpha = 3.2$. These two models also produced a reasonable good fit in Diego et al. (2001). In the above plot we have assumed $h = 0.75$ in L_o which was the value adopted in Babul et al. (2002). All the models represented in this plot give a reasonable fit to the observed $L_x - T$ relation (see figure 5 in Babul et al. 2002).

6.1 Preheating and the $L_x - T$ relation

In figure 13 we present some of the estimates of the $L_x - T$ relation used in this work compared to a model including pre-heating (solid line, Babul et al. 2002). All the models represented in the plot make a good fit to the most recent estimations of the $L_x - T$ relation (see e.g. Markevitch 1998, Allen & Fabian 1998, Helsdon & Ponman 2000). The pre-heating model corresponds to an entropy floor of $kT n_e^{-2/3} \approx 427 \text{keV cm}^2$. This pre-heated model gives an excellent match to the observations (see Babul et al. 2002). The model used in section 4 corresponds to the dashed line. The dotted line and dot-dashed line were used in section 5 to illustrate the change in the cluster power spectrum when the parameters L_o and α were changed. The main difference between the pre-heated model and the single scaling relation is that at temperatures $T \approx 1 \text{keV}$ the pre-heated models predict a larger luminosity than the standard single scaling relations. Clusters with T of a few keV correspond to intermediate masses. We have seen that this range of masses dominate the power spectrum so we should expect some kind of dependence on the power spectrum with the amount of entropy in the pre-heated model. As shown in Babul et al (2002), lower entropy floors will produce a larger shift of the relation to higher X-ray luminosities (lower α) while higher entropy floors will result in a steeper $L_x - T$ relation (higher α). At kT below 1 keV the situation inverts and the pre-heated model predicts clusters to be less luminous than in the single scaling case. Previous studies based on the intensity of the soft X-ray background suggest that there must be some level of pre-heating on galaxy clusters, for example

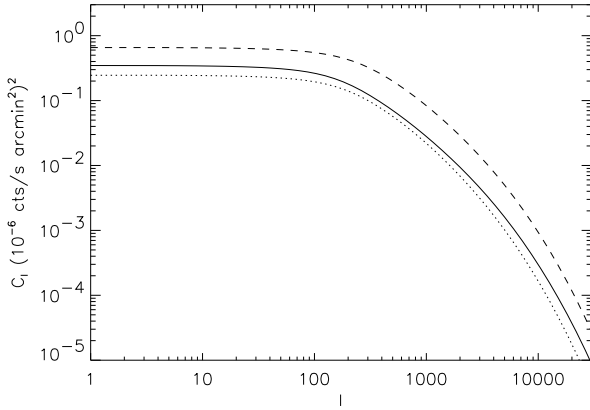


Figure 14. Change in power when pre-heating is considered. The solid line is the reference model ($\sigma_8 = 0.8$, $\Omega_m = 0.3$, $L_o = 1.12 \times 10^{42} h^{-2} \text{erg/s}$, $\alpha = 3.2$ and $\psi = 0.0$). In the reference model the temperature of the cluster is computed from the $T - M$ relation obtained in Diego et al. (2001) ($T(\text{keV}) = 9.48 M_{15}^{0.75} (1+z)$). The dashed line shows the power spectrum when the X-ray luminosity is computed from the pre-heating model (Babul et al. 2002) shown in figure 13 and the temperature is obtained from a numerical fit to the $T - M$ relation (Nevalainen et al. 2000), $T(\text{keV}) \approx 8.0 M_{15}^{0.56}$. For reference (dotted curve), we also show the cluster X-ray power spectrum when we use the Nevalainen et al. (2000) $T - M$ relation but the non-preheated model is used to get the X-ray luminosity (i.e. $L_o = 1.12 \times 10^{42} h^{-2} \text{erg/s}$ and $\alpha = 3.2$ for all T)

from AGN heating of the intracluster gas. Otherwise, their contribution to the soft to X-ray background exceeds the derived upper limit (see e.g. Wu et al. 2001). In figure 14 we show how the preheating can change the power spectrum of clusters. The solid line is the non-preheated model used in section 4 but with non-evolving $L_x - T$ ($\psi = 0$) (dashed line in figure 13). When we use the pre-heated model of Babul et al. (2002) (solid line in figure 13) we see an increase in the power spectrum by a factor of ≈ 2 (dashed line). In the pre-heated model case we also have computed the temperature of the cluster (from its mass) using a numerical fit to the observed $T - M$ relation (Nevalainen et al. 2000). That fit differs from the best-fitting $T - M$ function found in Diego et al. (2001). The Nevalainen’s $T - M$ relation is in perfect agreement with the latest estimate of the $T - M$ scaling (Shimizu et al. 2002) where the authors find $kT(\text{keV}) = 7.7 M_{15}^{0.55}$ (M_{15} is expressed in $10^{15} h^{-1} M_\odot$). It is also in agreement with previous results which suggest that the $T - M$ scaling relation differ from the expected self-similar behaviour (Mohr et al. 1999). When we use Nevalainen’s $T - M$ (but keeping the rest of parameters of the model corresponding to the solid line in figure 14) the new power spectrum changes from the solid line to the dotted line.

If we assume that the pre-heating model used above is a good description of the $L_x - T$ relation, we can extract some surprising conclusions. Our upper limits exclude many of the previous constraints on this parameter (see Refregier et al. 2002b for a recent compilation of constraints on σ_8). From the results compiled in Refregier et al. (2002b), only the

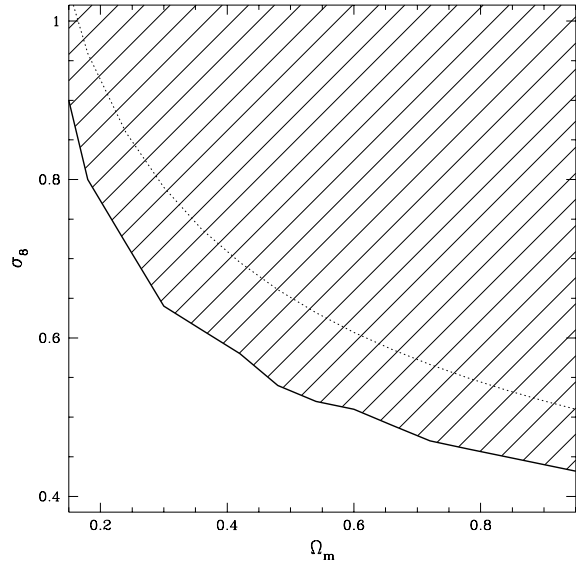


Figure 15. $\sigma_8 - \Omega_m$ constraints assuming the pre-heating model of Babul et al. (2002) and the $T - M$ relation of Nevalainen et al. (2000), (thick solid line). This upper limit would exclude models like $\sigma_8 = 0.8$, $\Omega_m = 0.3$. For reference we also show the result obtained in section 4 (dotted line).

recent 2dF+CMB (Lahav et al. 2001) and galaxy clusters (Seljak 2002) constraints are well inside our upper limits. This can have two interpretations. The first interpretation is that those constraints derived using other methods which are in contradiction with the RASS upper limit on σ_8 need to be revised with respect to the assumptions made in the appropriate analyses. The second interpretation is that we are being too optimistic in our assumptions. The assumed $L_x - T$ relation is not a good description of the underlying $L_x - T$ relation in galaxy clusters and we may need to *inject* more entropy in the clusters in order to make them less luminous (or any other mechanism which decreases the X-ray luminosity). This second interpretation is interesting because it shows us how we can study cluster physics if we know something about the cosmological model. If we assume that the underlying cosmological model can be described by the parameters $\sigma_8 = 0.8$ and $\Omega_m = 0.3$ (in a flat Λ CDM universe with $\Gamma = 0.2$) then we can ask whether or not the assumed physics ($L_x - T$ relation) is in agreement with the observations. We can test this by imposing that the theoretical power spectrum must be below the observed one.

6.2 $L_x - T$ and $T - M$ from $\sigma_8 - \Omega_m$

Although there is still a very lively debate about the value of σ_8 , there is a general consensus in the allowed range for σ_8 , $\sigma_8 \in (0.7 - 1.1)$ for $\Omega_m = 0.3$ with a most favoured value of $\sigma_8 \approx 0.8$. The fact that the preheating model considered above is excluding this most favoured value can have a simple interpretation, which is that our assumptions about the luminosities of the clusters are too optimistic. The clusters must be less luminous than we assumed in order to allow the upper limit to stay above the preferred value of

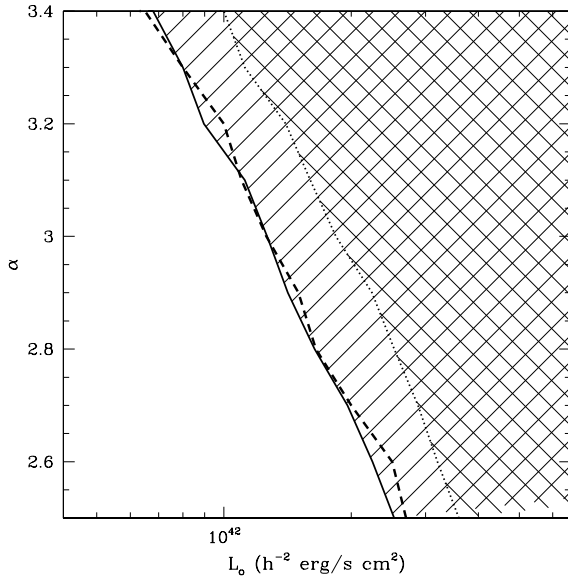


Figure 16. Upper limits on the value of L_o as a function of α for a cosmological model with $\sigma_8 = 0.8$ and $\Omega_m = 0.3$. The solid line mark the upper limits when we assume $T = 8.5M_{15}^{0.54}$ (Nevalainen et al. 2000). If the assumed $T - M$ relation is $T = 8.0M_{15}^{2/3}$ (Evrard et al. 1996) the upper limits on L_o change (dotted line). We also show the case when a pre-heating like model with two different exponents is assumed (dashed line), $L_x = L_o * T^\alpha$ for $T > 1$ keV and $L_x = L_o * T^\beta$ for $T < 1$ keV. We assumed $\beta = 2\alpha$ and the Nevalainen et al. (2000) $T - M$ relation. This shows how the constraints are not very sensitive to clusters with $T < 1$ keV.

σ_8 . If we parametrise the luminosity as $L_x = L_o T^\alpha$, then we can constrain L_o as a function of α by just requiring that the cluster power spectrum stays below the measured power spectrum (see figure 16). Although we have not discussed much about the $T - M$ relation, it will also play a role in the definition of the upper limit. To get the temperature in the $L_x - T$ relation we need to assume some form for $T - M$ relation. Recent observations (Nevalainen et al. 2000), seem to indicate that this relation differs slightly from the self similar scaling relation. However, as in the case of the $L_x - T$, there is some scattering on the $T - M$ relation. We have included this uncertainty into our calculations by using two different $T - M$ relations. In the first case we use the fit to the observed T and M obtained by Nevalainen et al. (2000), $T = 8.5M_{15}^{0.54}$ keV and in the second case we use a self-similar form (Evrard et al. 1996), $T = 8.0M_{15}^{2/3}$ keV. The results on L_o and α are shown in figure 16.

When we compare the models on the two upper limit curves with the observed $L_x - T$ relation (figure 17), we find that the models on the upper limits are marginally consistent with the observations. The model with the self-similar $T - M$ relation produces a constrain which agrees better with the observations.

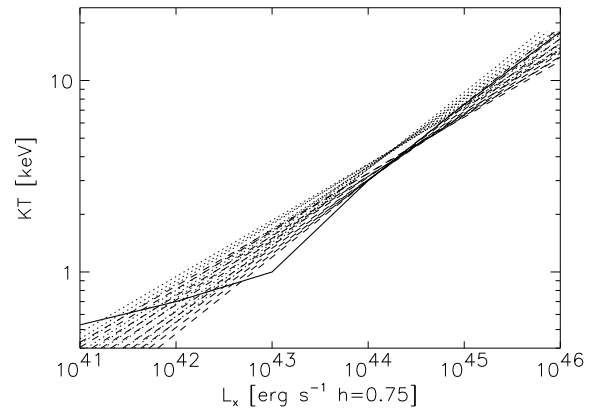


Figure 17. $L_x - T$ relations for the models lying in the two upper limits of figure 16. The dotted line corresponds to the models in the solid line of figure 16 while the dashed lines correspond to the models in the dotted line curve in figure 16. The solid line shows the preheating model of Babul et al. (2002).

7 DISCUSSION

We have found that in order to explain most of the constraints obtained in σ_8 and Ω_m , we need a rather steep $L_x - T$ relation. We have changed these relations within the observed limits (and even more, in the case of the parameter α) and we found that the $\sigma_8 = 0.8$ $\Omega_m = 0.3$ model can be accommodated only in the most extreme cases. Using the pre-heating model of Babul et al. (2002), our upper limit excludes most of the current constraints in σ_8 for $\Omega_m = 0.3$. If $\sigma_8 > 0.8$ for $\Omega_m = 0.3$, we may say that there is an inconsistency between the above preheating model and the upper limit imposed by the RASS diffuse background.

As noted by Voit et al. (2002), the observed $L_x - T$ relation changes when the luminosities are corrected by cooling flow effects. Our results suggest that cooling flows can be important (specially at low redshift which is the range dominating the power spectrum in this scale). A $L_x - T$ which is obtained without correcting for cooling flows will be affected by a larger scatter due to the presence of the clusters with cooling flows (they will increase the average luminosity of clusters and therefore the value of L_o). If cooling flow clusters are not representative of the average population of clusters, they should be excluded from any fit to the $L_x - T$ relation or corrected their luminosities (and average temperatures) by the effect of the cooling flow in order to get a representative $L_x - T$ relation (see Fabian et al. 1994 for a discussion on the effect of cooling flows in the $L_x - T$ relation).

In figure 18 we present one of the *extreme* cases for which the model $\sigma_8 = 0.8$, $\Omega_m = 0.3$ is just below the upper limit (solid line). This model corresponds to the values $L_o = 2.3 \times 10^{42} h^{-2} \text{ erg s}^{-1}$ and $\alpha = 3$ and is in the dotted curve of figure 16 (i.e. when we assume the self-similar relation $T = 8.0M_{15}^{2/3}$ keV). If we compare this extreme case with real observations of the $L_x - T$ relation, we see that this model still produces a good fit to the data (but we need to assume that $T \propto M_{15}^{2/3}$). All the models lying on the right hand

side of the solid line overpredict the observed RASS power spectrum for $\sigma_8 = 0.8$, $\Omega_m = 0.3$. The pre-heating model of Babul et al. (2002) (bottom dotted line) is marginally consistent with the upper limit above 4 keV but exceeds the upper limit below that temperature. On the other hand, the pre-heated model of Voit & Bryan (2001) is still compatible with the upper limit but is well within the limits. There is little room for additional changes in the $L_x - T$ and $T - M$ relation without coming into serious contradictions with the observed relations. As a consequence, our results suggest that it is very difficult to accommodate high σ_8 models ($\sigma_8 \geq 0.8$) within our upper limit. Recently, a combined analysis of 2dF plus CMB data has produced new constraints on σ_8 which suggest that $\sigma_8 \approx 0.7$ for $\Omega_m h = 0.21$ (no tensor model) and $\sigma_8 \approx 0.6$ for $\Omega_m h = 0.16$ (tensor model) (see Efstathiou et al. 2002). Other recent works also suggest a low value for σ_8 (e.g Allen et al. 2002, Seljak 2002, Bahcall et al. 2002). These values of σ_8 are in very good agreement with our upper limits. If the value of σ_8 is significantly larger than 0.8, (for $\Omega_m = 0.3$) then, we can conclude that there is a serious contradiction between the X-ray data and the model. If we adopt the *realistic* position that the inconsistency must be in the model, then, we should revise our assumptions in order to resolve this puzzling situation.

The only assumption we have not checked in our model is that about the mass function. As mentioned in the introduction, the modelling of the cluster power spectrum involves the whole population of clusters. This fact makes the cluster power spectrum a very sensitive probe of the cluster mass function.

This opens the exciting possibility of (assuming the cosmological model is known) constraining the cluster mass function once we know accurately the $L_x - T$ and $T - M$ relations and a good estimation of the X-ray background power spectrum is available.

There is an important point which has not been explored in this paper but that we plan to study in a subsequent work. It is the scattering of the $L_x - T$ relation. Real clusters will show an intrinsic scattering in this relation (clusters with the same temperature may have different luminosities around the *average* L_x). Since the power spectrum of clusters is proportional to the square of the multipole decomposition (equations. 1 and 3), those clusters with the same T but L_x larger than the mean will contribute more to the power spectrum than the clusters with L_x lower than the mean (but the same T). That is, the *average* effect of the population of clusters with the same T (but different L_x) is not the same as the effect of the population of clusters with the same T and *average* luminosity L_x (due to the quadratic dependence of C_l). This fact may change the results presented in this work and need to be studied in more detail.

8 CONCLUSION

We have shown that the use of the measured X-ray power spectrum as an upper limit produces strong constraints on the cosmological model. The constraints have the advantage of being very robust since they were obtained under a minimum number of assumptions. The uncertainty in the

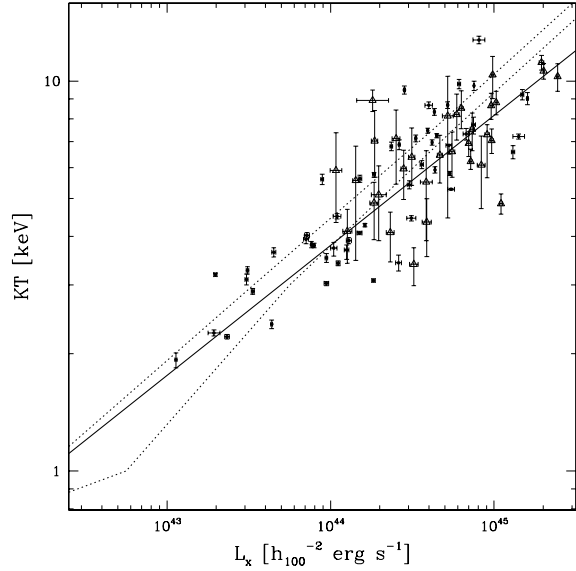


Figure 18. Scaling model for the curve in the upper limit $L_o = 2.310^{42} h^{-2} \text{erg/s}$ and $\alpha = 3$ (solid line). The model is compared with a recent compilation of temperatures and luminosities (Novicki et al. 2002) at low (dots) and intermediate redshift (open triangles). The two dotted lines show the preheating models of Voit & Bryan (2001) (top) and Babul et al. (2002) (bottom). Note the large scattering in the data.

Figure 19. Upper limit on $\sigma_8 - \Omega_m$ compared with a recent constraint in these parameters from CMB (Melchiorri et al. 2002). The X-ray background upper limit excludes half of the CMB constraints.

assumptions can be easily incorporated into the model to produce optimistic and pessimistic constraints. Approaches like the one presented in this work are needed to complement the constraints obtained using other methods (see figure 19). To obtain the upper limits on $\sigma_8 - \Omega_m$ presented in this work we do not even need to detect the clusters. The global contribution of all the clusters (above or below the 3σ level) contributes to the power spectrum although we have seen that the cluster population with intermediate masses and $z < 0.2$ dominates the power spectrum in the range of scales considered in this work.

In this work, we have not considered the clustering contribution (two-halo). This contribution may be of the order of 20% – 30% at the scales relevant for this work (Lahav et al. 1997, Komatsu & Kitayama 1999). The upper limits presented here will be even more significant if this contribution is incorporated into the analyses.

Due to the point source contamination and large pixel size, the constraints on $\sigma_8 - \Omega_m$ arise in the range $l < 100 - 200$. However, this fact has an advantage. At low l 's, the cluster power spectrum is independent of the electron density profile (or the internal structure of the cluster) and only the total luminosity of the clusters matters for modelling the power spectrum. This reduces dramatically the number of

assumptions made in the model. One may use this fact to make studies of the physics of the intracluster plasma (like pre-heating) which could constrain the $L_x - T$ relation.

We found that, in order to accommodate cosmological models like $\sigma_8 = 0.8$ $\Omega_m = 0.3$ we need to *tune* the $T - M$ and the $L_x - M$ relation to the limits of the observational constraints. This fact suggest that lower σ_8 models are favoured by the upper limit constraint set by the X-ray background.

The approach presented in this work can be extremely useful with higher resolution and better signal to noise data (*Chandra*, and particularly XMM-Newton). Although the data in the *ROSAT* R6 band has the brightest point sources removed, the power spectrum still contains some contribution coming from the non-removed point sources and their clustering. Future data from *Chandra* and specially XMM-Newton will allow a better point source subtraction. The constraints obtained from these new data will be much more significant since one can probe smaller scales with a significantly smaller contamination from point sources. In the small scale range, the cluster power spectrum becomes even more sensitive to the physics of the plasma (angular extension of the emission and evolution of the $L_x - T$ relation). In particular, we have seen that the shape of the power spectrum at small scales (large multipoles) is better described by density profiles having high clumpiness factors ($p \approx 10 - 20$). A low-contaminated point source power spectrum could lead to dramatic constraints on the $L_x - T$ relation. These constraints can have serious implications for the physics of the intracluster plasma (pre-heating, cooling flows). These facts make worth extending the analyses presented here to smaller scales with a high sensitivity where the point source removal can be performed to very low fluxes.

9 ACKNOWLEDGEMENTS

This research has been supported by a Marie Curie Fellowship of the European Community programme *Improving the Human Research Potential and Socio-Economic knowledge* under contract number HPMF-CT-2000-00967. XB acknowledges financial support from the Spanish Ministry of Science and Technology under project AYA2000-1690. The authors would like to thank Wayne Hu, Greg Bryan and Francisco Carrera for fruitful discussions. We also thank A. Melchiorri for providing the plot with the confidence levels derived from CMB.

REFERENCES

- Allen S.W., Fabian A.C., 1998, MNRAS, 297, 57.
 Allen S.W., Schmidt R.W., Fabian A.C., Ebeling H., 2002, MNRAS submitted. Preprint astro-ph/0208394.
 Arnaud K.A., 1996, *Astronomical Data Analysis Software and Systems V*, eds. Jacoby G. and Barnes J., p17, ASP Conf. Series, volume 101.
 Atrio-Barandela F., & Mucket J.P., 1999, ApJ, 515:465.
 Babul A., Balogh M.L., Lewis G.F., Poole G.B., 2002, MNRAS, 330, 329.
 Bahcall N.A., Fan X., 1998, ApJ, 504, 1.
 Bahcall N.A., et al. (more than 8 authors), 2002 ApJ submitted, astro-ph/0205490.
 Barcons X., Fabian A.C., 1988, MNRAS, 230, 189.
 Barcons X., Fabian A.C., Carrera F., 1998, MNRAS, 293, 60.
 Bartlett J.G., & Silk J., 1994, ApJ, 423, 12.
 Borgani S., Plionis M., Kolokotronis V., 1999, MNRAS, 305, 866.
 Carrera F.J., Fabian A.C., Barcons X., 1997, MNRAS, 285, 820.
 Cole S., & Kaiser N., 1988, MNRAS, 233, 637.
 Cooray A., 2002, ApJ, 576, 105.
 Diego J.M., Martínez-González E., Sanz J.L., Cayón L., Silk J. 2001, MNRAS, 325, 1533.
 Efstathiou et al. (more than 8 authors). 2002, MNRAS, 330, L29.
 Evrard A.E., Metzler C.A., Navarro J.F., 1996, ApJ, 469, 494.
 Fabian A.C., Barcons X., 1992, ARA&A, 30, 429.
 Fabian A.C., Crawford C.S., Edge A.C., Mushotzky R.F. 1994, MNRAS, 267, 779.
 Heldson S.F., Ponman T.J., 2000, MNRAS, 315, 356.
 Kneissl R., Egger R., Hasinger G., Soltan A.M., Trümper J., 1997, A&A, 320, 685.
 Komatsu E., & Kitayama T., 1999, ApJ, 526, L1.
 Komatsu E., & Seljak U., T., 2002, MNRAS, 336, 1256.
 Lahav O., Piran T., Treyer M., 1997, MNRAS, 284, 499.
 Lahav O., et al. 2001. MNRAS submitted. astro-ph/0112162.
 Markevitch M., 1998, ApJ, 504, 27.
 Melchiorri A., Bode P., Bahcall N.A., Silk J., 2002, astro-ph/0212276.
 Miyaji T., Hasinger G., Egger R., Trümper J., Freyberg M.J., 1996, A&A, 312, 1.
 Mohr J.J., Mathiesen B., Evrard A.E., 1999, ApJ, 517, 627.
 Nevalainen J., Markevitch M., Forman W., 2000, ApJ, 532, 694.
 Novicki M.C., Sornig M., Henry J.P. 2002, AJ, 124,2413.
 Percival W.J., et al. (more than 8 authors) 2001, MNRAS, 327, 1297.
 Press W.H., Schechter P., 1974, ApJ, 187, 425.
 Refregier A., Valtchanov I., Pierre M. 2002a, A&A, 390, 1.
 Refregier A., Rhodes J., Groth E., 2002b, ApJ, 572, 131.
 Reiprich T.H., Böhringer H. 2002, ApJ, 567, 716.
 Schuecker P., Böhringer H., Guzzo L., Collins C.A., Neumann D.M., Schindler S., Voges W., De Grandi S., Chincarini G., Cruddace R., Müller V., Reiprich T.H., Retzlaff J., Shaver P. 2001, A&A, 368, 86.
 Schuecker P., Guzzo L., Collins C.A., Böhringer H. 2002, MNRAS, 335, 807.
 Seljak U., 2002, MNRAS in press. astro-ph/0111362.
 Shimizu M., Kitayama T., Sasaki S., Suto Y. 2002, ApJ in press. Preprint astro-ph/0212284.
 W. Sliwa, A.M. Soltan, & M.J. Freyberg. 2001, A&A, 380, 397.
 Snowden S.L., Egger R., Freyberg M.J., McCammon D., Plucinsky P.P., Sanders W.T., Schmitt, J. H.M.M., Truemper J., Voges W. 1997, ApJ, 485, 125.
 Soltan A.M., Hasinger G., Egger R., Snowden S., Trümper J., 1996, A&A, 305, 17.
 Treyer M., Scharf C., Lahav O., Jahoda K., Boldt E., Piran T., 1998, ApJ, 509, 531.
 Viana P.T.P., Nichol R.C., Liddle A.R. 2002, ApJ, 569, 75.
 Voges W., et al. (more than 8 authors), 1999, A&A 349, 389-405
 Voges W., et al. (more than 8 authors), 2000, IAUC, 7432.
 Voit G.M., Bryan G.L., Balogh M.L., Bower R.G., 2002, ApJ, 576, 601.
 Voit G.M. & Bryan G.L., 2001, Nature, 414, 425.
 White M., 2001, MNRAS, 321, 1.
 Wu K.K.S., Fabian A.C., Nulsen P.E.J., 2001, MNRAS, 324, 95.
 Yamamoto K., Sugiyama N., 1998, PhRevD, 58, 103508.

This paper has been produced using the Royal Astronomical Society/Blackwell Science L^AT_EX style file.

This figure "Figure1.gif" is available in "gif" format from:

<http://arxiv.org/ps/astro-ph/0302067v1>

This figure "Figure19.gif" is available in "gif" format from:

<http://arxiv.org/ps/astro-ph/0302067v1>